Creating Ferroelectricity in Monoclinic $(HfO_2)_1/(CeO_2)_1$ Superlattices

Hong Jian Zhao,[1,2,3] Yuhao Fu,[1] Longju Yu,[1] Yanchao Wang,[1,4,*] Yurong Yang,[5] Laurent Bellaiche,[6] and Yanming Ma[1,3,4,†]

[1]*Key Laboratory of Material Simulation Methods and Software of Ministry of Education, College of Physics, Jilin University, Changchun 130012, China*

[2]*Key Laboratory of Physics and Technology for Advanced Batteries (Ministry of Education), College of Physics, Jilin University, Changchun 130012, China*

[3]*International Center of Future Science, Jilin University, Changchun 130012, China*

[4]*State Key Laboratory of Superhard Materials, College of Physics, Jilin University, Changchun 130012, China*

[5]*National Laboratory of Solid State Microstructures and Jiangsu Key Laboratory of Artificial Functional Materials, Department of Materials Science and Engineering, Nanjing University, Nanjing 210093, China*

[6]*Smart Ferroic Materials Center, Physics Department and Institute for Nanoscience and Engineering, University of Arkansas, Fayetteville, Arkansas 72701, USA*

(Received 16 October 2023; accepted 16 May 2024; published 17 June 2024)

Ferroelectricity in CMOS-compatible hafnia (HfO_2) is crucial for the fabrication of high-integration nonvolatile memory devices. However, the capture of ferroelectricity in HfO_2 requires the stabilization of thermodynamically metastable orthorhombic or rhombohedral phases, which entails the introduction of defects (e.g., dopants and vacancies) and pays the price of crystal imperfections, causing unpleasant wake-up and fatigue effects. Here, we report a theoretical strategy on the realization of robust ferroelectricity in HfO_2-based ferroelectrics by designing a series of epitaxial $(HfO_2)_1/(CeO_2)_1$ superlattices. The designed ferroelectric superlattices are defects free, and most importantly, on the base of the thermodynamically stable monoclinic phase of HfO_2. Consequently, this allows the creation of superior ferroelectric properties with an electric polarization $> 25\ \mu C/cm^2$ and an ultralow polarization-switching energy barrier at ~ 2.5 meV/atom. Our work may open an avenue toward the fabrication of high-performance HfO_2-based ferroelectric devices.

DOI: 10.1103/PhysRevLett.132.256801

Introduction.—Discovering ferroelectrics that are compatible with CMOS is crucial for fabricating high-integration nonvolatile memory devices [1,2]. The hafnia (HfO_2) that is extensively used in CMOS devices [1] became one such material since the finding of ferroelectricity in Si-doped HfO_2 [3]. However, the ferroelectric phases of HfO_2 are thermodynamically metastable over a broad temperature range (e.g., from 0 °C to 1500 °C) and at ambient pressure—the stable phase being the monoclinic $P2_1/c$ phase, which is paraelectric [4]. So far, the strategies for realizing ferroelectricity in HfO_2 mostly rely on the introduction of defects (e.g., dopants and vacancies) under special fabrication conditions (e.g., suitable film thickness and epitaxial strain) [1,5–14]. The role of crystal defects is to either stabilize the metastable ferroelectric phases (being orthorhombic or rhombohedral) [6,7] or induce the ferroelectricity in the monoclinic phase [8,14]. Such strategies yielded the fabrication of various HfO_2-based ferroelectrics, represented by Y-doped HfO_2 [15–18], La-doped HfO_2 [19–21], $Hf_{1-x}Ce_xO_2$ [22–26], $Hf_{0.5}Zr_{0.5}O_2$ [27–33], HfO_2/ZrO_2 superlattices [34–36], and $Hf(Zr)_{1+x}O_2$ [37] with orthorhombic $Pca2_1$ or rhombohedral $R3m$ space group. However, these resulting materials often suffer from imperfections such as crystal defects and mixed nonferroelectric phases (see e.g., Ref. [1]). Such imperfections are detrimental to the ferroelectric cycling stabilities in HfO_2-based ferroelectrics, causing wake-up and fatigue effects [1,8,38,39].

Having a new strategy to design robust ferroelectricity in HfO_2-based compounds is therefore highly desirable and timely. Here, we explore the possibility for engineering ferroelectricity in defect-free monoclinic HfO_2 by symmetry analysis and first-principles simulations. We show that such ferroelectricity can, in fact, be achieved by creating the $(HfO_2)_1/(CeO_2)_1$ superlattices, where Hf and Ce ions are appropriately ordered. Unlike the previously reported HfO_2-based ferroelectrics, our proposed ferroelectricity in $(HfO_2)_1/(CeO_2)_1$ superlattices originates from the thermodynamically stable $P2_1/c$ phase of HfO_2 and its natural evolution into a ferroelectric state via nanostructuring. Engineering ferroelectricity in these superlattices is thus guaranteed and results in defect-irrelevant HfO_2-based ferroelectrics with superior ferroelectric properties.

Creating ferroelectricity in the monoclinic phase.—The lattice parameters (a, b, c) of the bulk $P2_1/c$ HfO_2—obtained by first-principles calculations—are (5.08, 5.16, 5.25) Å, where a, b, and c are along the [100], [010], and

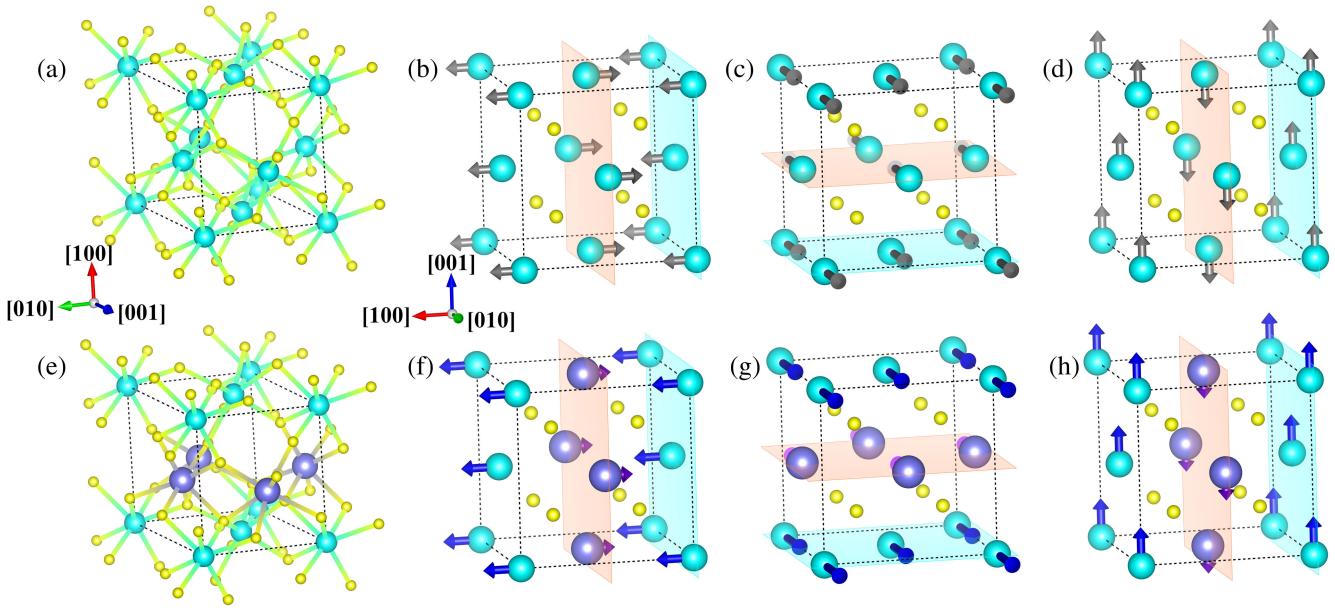

FIG. 1. (a) Schematization of the $P2_1/c$ phase of HfO_2. (b)–(d) Three antipolar motions of Hf ions in the $P2_1/c$ phase of HfO_2. (e) The [100]-oriented $(HfO_2)_1/(XO_2)_1$ superlattice obtained by replacing a sequence of Hf ions (of the $P2_1/c$ HfO_2 oxide) by X ions; such replacements are ordered with respect to the (100) crystallographic plane. In reality, the positions of Hf, X, and O in the $(HfO_2)_1/(XO_2)_1$ superlattice will be adjusted, compared with those of Hf and O in $P2_1/c$ HfO_2. In (e), we merely sketch the formation of the [100]-oriented $(HfO_2)_1/(XO_2)_1$ superlattice (from $P2_1/c$ HfO_2), without demonstrating the adjustments of the ionic positions. (f),(h) The atomic displacements in the [100]-oriented $(HfO_2)_1/(XO_2)_1$ superlattice. (g) The atomic displacements in the [001]-oriented superlattice. The Hf, X, and O ions are represented by cyan, purple, and yellow spheres, respectively. The displacements of Hf or X ions are denoted by gray, blue, or purple arrows—the displacements of O being not shown. In (a) and (e), the [100] and [001] axes form a non-90° monoclinic angle; in (b)–(d) and (f)–(h), the [100], [010], and [001] axes are perpendicular to each other.

[100] crystallographic directions, respectively [see Fig. 1(a)]. The [100] and [001] directions exhibit a monoclinic angle of ~99.6°. Symmetry analysis indicates that the Hf sublattice in this $P2_1/c$ phase presents three types of antipolar motions [see Figs. 1(b)–1(d)], compared with the high-symmetric $Fm\bar{3}m$ phase [40]. In these motions, we can identify two types of crystallographic planes, colored cyan and orange in Figs. 1(b)–1(d). The Hf ions within the cyan or orange plane are displaced along the same direction, while those between the cyan and orange planes are moved oppositely. In Fig. 1(b), we depict one antipolar motion involving the displacements of Hf ions along [100] and $[\bar{1}00]$ directions. The Hf ions displaced along [100] and those displaced along $[\bar{1}00]$ are stacked along the crystallographic [100] direction. More vividly, the cyan and orange planes in Fig. 1(b) are alternately aligned along the crystallographic [100] orientation. In the same stacking mode, the displacements of Hf ions can also occur along [001] and $[00\bar{1}]$ orientations [see Fig. 1(d)]. Besides, the $P2_1/c$ phase exhibits another antipolar motion [see Fig. 1(c)], where the displacements of Hf ions are along [010] and $[0\bar{1}0]$ orientations and the stacking (of the [010]-displaced and $[0\bar{1}0]$-displaced Hf ions) is occurring along the crystallographic [001] direction. In these three cases, the overall displacements of Hf ions along opposite directions are identical in magnitude, compensating with each other (i.e., no electric polarization).

To engineer ferroelectricity in $P2_1/c$ phase of HfO_2, a possible strategy is to create the $(HfO_2)_1/(XO_2)_1$ superlattice with X being different from Hf. In this superlattice, the Hf and X ions should be stacked in such a way that Hf and X ions are displaced along $\pm\alpha$ and $\mp$ α directions (α being [100], [010], or [001]) [41], respectively [see Figs. 1(f)–1(h)]. Essentially, the $(HfO_2)_1/(XO_2)_1$ superlattices can be obtained via the replacements of some specific Hf ions in $P2_1/c$ HfO_2 by X ions, as exemplified by Fig. 1(e). Under these circumstances, the Hf and X ions are displaced, albeit oppositely, with noncompensated magnitudes, yielding net off-center displacements and an electric polarization.

As shown in Figs. 1(f) and 1(h), the [100]-oriented $(HfO_2)_1/(XO_2)_1$ superlattice [42] allows electric polarization along $\pm$[100] and $\pm$[001] directions. Figure 1(g) sketches the displacements of Hf and X ions in the [001]-oriented $(HfO_2)_1/(XO_2)_1$ superlattice. This superlattice gains an electric polarization along $\pm$[010] direction. As for the [010]-oriented superlattice, no net off-center displacements can be expected. Our aforementioned arguments are confirmed by the symmetry analysis: the [100]- and [001]-oriented $(HfO_2)_1/(XO_2)_1$ superlattices exhibit Pc and $P2_1$ space groups, respectively, both of which are compatible with ferroelectricity. The [010]-oriented $(HfO_2)_1/(XO_2)_1$ superlattice, on the other hand, is centrosymmetric and nonferroelectric. Our strategy for engineering

ferroelectricity in $(HfO_2)_1/(XO_2)_1$ superlattice can basically be linked with the notion of hybrid improper ferroelectricity that was previously developed to describe the ferroelectricity in perovskites superlattices and Ruddlesden-Popper compounds [43–46].

Energetics of the $(HfO_2)_1/(CeO_2)_1$ *superlattices.*—Our aforementioned discussion suggests that stabilizing the [100]- or [001]-oriented $(HfO_2)_1/(XO_2)_1$ superlattice is the key to engineering ferroelectricity in it. In view of this, we decide to find appropriate XO_2 oxide so that it can combine with $P2_1/c$ HfO_2 and form the [100]- or [001]-oriented superlattice. We recall that the $P2_1/c$ HfO_2 can be seen as the derivative of the fluorite-type $Fm\bar{3}m$ HfO_2 [1]. Finding another fluorite-type XO_2 oxide will be the design principle for our aforementioned $(HfO_2)_1/(XO_2)_1$ superlattices. Searching the Materials Project database [47,48] and following Ref. [2], we identify CeO_2 and ZrO_2 as the candidates for XO_2. We first explore the ferroelectricity in $(HfO_2)_1/(CeO_2)_1$ superlattice, and move to the $(HfO_2)_1/(ZrO_2)_1$ superlattices at a later stage. The CeO_2 oxide is fluorite-structured with the $Fm\bar{3}m$ space group [49] over a wide temperature spectrum (e.g., from 0 °C to 2500 °C) [50–52]. Earlier work shows that CeO_2 can form solid solutions with HfO_2, yielding HfO_2-based ferroelectrics (see, e.g., Refs. [22–26]). The shared prototype structure (i.e., fluorite type) of $P2_1/c$ HfO_2 and $Fm\bar{3}m$ CeO_2 implies the possibility for achieving the $(HfO_2)_1/(CeO_2)_1$ superlattice. Experimentally, this kind of short-period superlattice can be epitaxially grown on appropriate substrates. To accommodate the [100]- or [001]-oriented $(HfO_2)_1/(CeO_2)_1$ superlattice, the cubic $\langle 100\rangle$-oriented substrate with appropriate in-plane lattice parameter a_{IP} may be selected for such epitaxial growth.

Now, we mimic the $(HfO_2)_1/(CeO_2)_1$ superlattice grown on various substrates (i.e., with various a_{IP}) by first-principles calculations. We examine the [100]-, [010]-, and [001]-oriented $(HfO_2)_1/(CeO_2)_1$ superlattices, since superlattices of these types can geometrically match the cubic $\langle 100\rangle$-oriented substrate. For each of the superlattices, we fix its in-plane lattice vectors to $(a_{IP}, 0, 0)$ and $(0, a_{IP}, 0)$, and relax its out-of-plane lattice vector and atomic positions. Figure 2(a) shows the energetics of the [100]-, [010]-, and [001]-oriented $(HfO_2)_1/(CeO_2)_1$ superlattices as a function of a_{IP}. The [100]-oriented $(HfO_2)_1/(CeO_2)_1$ superlattice is more stable than the [010]- and [001]-oriented cases over a broad a_{IP} range (e.g., from 5.24 to 5.34 Å) [53]. These in-plane lattice parameters correspond to (i) compressive strains ranging from −3.0% to −1.1% with respect to 5.40 Å of bulk $Fm\bar{3}m$ CeO_2, and (ii) tensile strains ranging from 0.8% to 2.7% with respect to $(b + c)/2 = 5.20$ Å of bulk $P2_1/c$ HfO_2. In particular, the [100]-oriented $(HfO_2)_1/(CeO_2)_1$ superlattice with $a_{IP} = 5.30$ Å roughly corresponds to the −1.9% compressively strained CeO_2 and the 1.9% tensilely strained HfO_2. Compared with their bulk phases, the HfO_2 and CeO_2 in the [100]-oriented $(HfO_2)_1/(CeO_2)_1$ superlattices are moderately strained. Such moderate strain conditions imply the possibility for growing the [100]-oriented $(HfO_2)_1/(CeO_2)_1$ superlattice epitaxially.

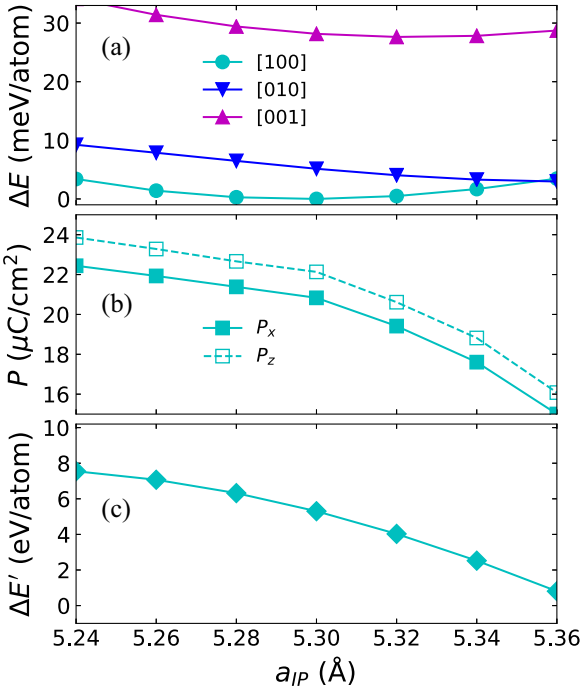

FIG. 2. Various physical quantities of the $(HfO_2)_1/(CeO_2)_1$ superlattice as a function of the in-plane lattice parameter a_{IP}. (a) The relative energy ΔE of the [100]-, [010]-, and [001]-oriented superlattices. (b) The electric polarization P of the [100]-oriented superlattices. (c) The polarization-switching energy barrier $\Delta E'$ for the [100]-oriented superlattices.

Landau theory for hybrid improper ferroelectricity in the $(HfO_2)_1/(CeO_2)_1$ *superlattices.*—Prior to studying the ferroelectric behaviors of the [100]-oriented $(HfO_2)_1/(CeO_2)_1$, we develop the Landau theory for describing the ferroelectricity in the $(HfO_2)_1/(CeO_2)_1$ superlattices. To this end, we start from the cubic $Fm\bar{3}m$ HfO_2 and create a tetragonal $(HfO_2)_1/(CeO_2)_1$ superlattice ($P4/mmm$ space group), where the Hf and Ce ions are ordered by layer along z direction [see Fig. 3(a)]. With respect to the tetragonal phase, we identify a sequence of nonpolar atomic motions that may be hosted by the [100]- and [001]-oriented $(HfO_2)_1/(CeO_2)_1$ superlattices. These motions are shown in Fig. S1 of the Supplemental Material (SM) [54]. Apart from these nonpolar motions, there are three polar motions in $(HfO_2)_1/(CeO_2)_1$ superlattices, namely, P_χ ($\chi = x, y, z$) being associated with the electric polarization along χ direction. These atomic motions exhibit a variety of trilinear couplings shown in Eq. (S1) of the SM. As for the [100]-oriented $(HfO_2)_1/(CeO_2)_1$ superlattice, symmetry analysis suggests the following atomic motions: $O_{100} \equiv (P_x, P_z, \Gamma_2^{5+}, M^{1-}, M^{2+}, M^{3+}, M^{4-}, M_y^{5-}, M_y^{5+})$, with the nonpolar motions schematized in Fig. 3. The trilinear couplings regarding the [100]-oriented

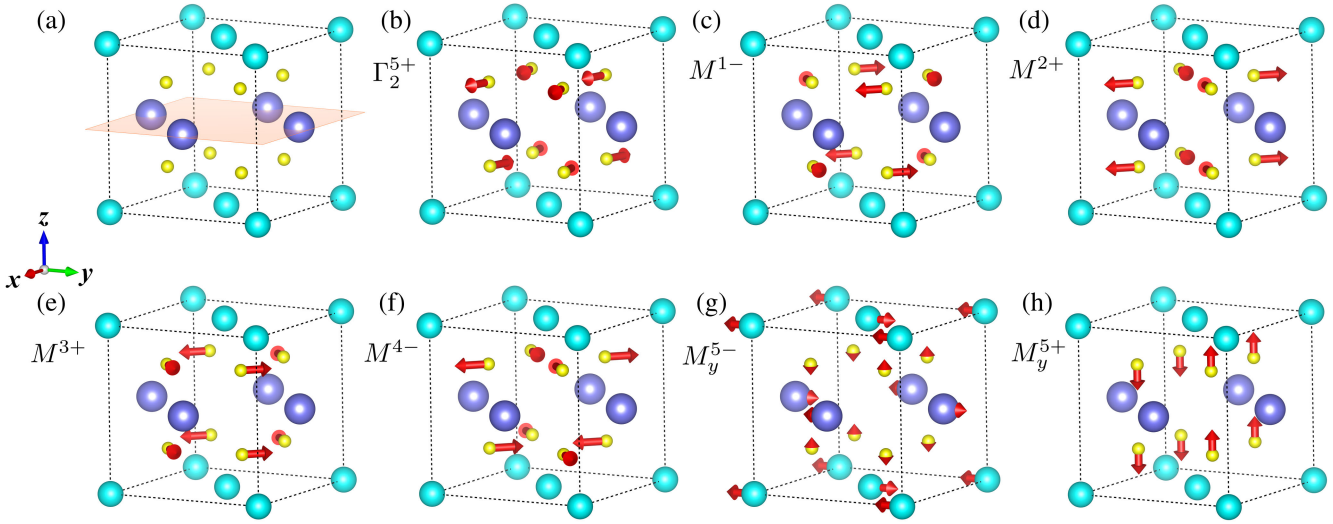

FIG. 3. The schematizations of the nonpolar atomic motions in the [100]-oriented $(HfO_2)_1/(CeO_2)_1$ superlattice (Pc space group). (a) The $P4/mmm$ reference phase of $(HfO_2)_1/(CeO_2)_1$. (b)–(h) The nonpolar atomic motions. The Hf, Ce, and O ions are denoted by cyan, purple, and yellow spheres. The Cartesian directions of our coordinate system are labeled by "x," "y," and "z." The crystallographic [100] direction in $P2_1/c$ HfO_2 roughly corresponds to the z axis. The atomic displacements are shown by red arrows. In the M_y^{5-} motion, the displacements contributed by Ce and O ions are negligible compared with those from Hf ions; for displaying clarity, we enlarge the magnitudes of Ce's and O's displacements in (g).

superlattice are $H_{100}=\alpha_1 M^{2+}M^{4-}P_z+\alpha_2 M^{3+}M^{1-}P_z+\alpha_3 M_y^{5-}M_y^{5+}P_z+\kappa P_x P_z \Gamma_2^{5+}+\beta_2 P_x M_y^{5-}M^{2+}+\beta_3 P_x M_y^{5-}M^{3+}+\beta_6 P_x M_y^{5+}M^{4-}+\beta_7 P_x M_y^{5+}M^{1-}+\lambda_3 \Gamma_2^{5+}M_y^{5-}M^{4-}-\lambda_4 \Gamma_2^{5+}M_y^{5-}M^{1-}+\lambda_7 \Gamma_2^{5+}M_y^{5+}M^{2+}-\lambda_8 \Gamma_2^{5+}M_y^{5+}M^{3+}$. Of particular interest are the couplings given by $H_{100}^{\mathrm{Polar}}=\alpha_1 M^{2+}M^{4-}P_z+\alpha_2 M^{3+}M^{1-}P_z+\alpha_3 M_y^{5-}M_y^{5+}P_z+\beta_2 P_x M_y^{5-}M^{2+}+\beta_3 P_x M_y^{5-}M^{3+}+\beta_6 P_x M_y^{5+}M^{4-}+\beta_7 P_x M_y^{5+}M^{1-}$. These terms are $P_\chi X_1 X_2$-type couplings (X_1 and X_2 being two nonpolar motions) and imply that the combination of X_1 and X_2 nonpolar motions leads to electric polarization P_χ. For instance, the coexistence of M^{2+} and M^{4-} nonpolar motions [see Figs. 3(d) and 3(f)] indicates the emergence of electric polarization along z direction, as suggested by the $\alpha_1 M^{2+}M^{4-}P_z$ term.

We move on to discuss the polarization switching path in the [100]-oriented $(HfO_2)_1/(CeO_2)_1$ superlattice. To this end, we take our aforementioned O_{100} state as our initial state, and identify the possible final states when switching the polarization from (P_x, P_z) to $(-P_x, -P_z)$. The H_{100} discussed above indicates that reversing the polarization will change some of the nonpolar motions and maintain others. This can be demonstrated as follows, taking $\alpha_2 M^{3+}M^{1-}P_z$ and $\beta_7 P_x M_y^{5+}M^{1-}$ terms as examples. The $\alpha_2 M^{3+}M^{1-}P_z$ term implies that reversing P_z will flip either M^{1-} or M^{3+} (but not both). Working with $\beta_7 P_x M_y^{5+}M^{1-}$, this causes two possible consequences: (i) if M^{3+} is not flipped (M^{1-} being flipped), M_y^{5+} will not be flipped either, and (ii) if M^{3+} is flipped (M^{1-} being not flipped), M_y^{5+} will be flipped as well. Furthermore, the $\kappa P_x P_z \Gamma_2^{5+}$ term implies that Γ_2^{5+} will be unchanged when switching (P_x, P_z) to $(-P_x, -P_z)$. Following this logic, we identify two possible final states O'_{100} and O''_{100} with respect to O_{100}. Apart from the reversed P_x and P_z, the O'_{100} state showcases reversed M^{2+}, M^{3+}, and M_y^{5+}, while the O''_{100} state exhibits reversed M^{1-}, M^{4-} and M_y^{5-}. The O'_{100} and O''_{100} final states suggest the O_{100}-O'_{100} and O_{100}-O''_{100} polarization switching paths for [100]-oriented $(HfO_2)_1/(CeO_2)_1$ superlattice [79].

Ferroelectricity in the [100]-oriented $(HfO_2)_1/(CeO_2)_1$ *superlattices.*—We move on to determine the polarization switching behavior for the [100]-oriented $(HfO_2)_1/(CeO_2)_1$ superlattice with $a_{\mathrm{IP}} = 5.30$ Å. Regarding this superlattice, the O_{100}-O'_{100} (respectively, O_{100}-O''_{100}) switching path indicates the intermediate $P2/c$ (respectively, $P2_1/c$) phase for polarization switching [80]. The energy barriers for the polarization switching via O_{100}-O'_{100} and O_{100}-O''_{100} paths are ~13.6 and ~77.2 meV/atom (see Fig. S4 of the SM), respectively, obtained by first-principles self-consistent calculations (without structural relaxations). The nudged elastic band (NEB) algorithm [81] further decreases the energy barrier (regarding the O_{100}-O'_{100} path) to ~5.3 meV/atom (see Fig. S4 of the SM). We also examine the effect of a_{IP} on the polarization-switching barrier in [100]-oriented $(HfO_2)_1/(CeO_2)_1$ superlattices [see Fig. 2(b)]. Varying a_{IP} from 5.24 to 5.34 Å reduces the barriers from ~7.5 to ~2.5 meV/atom. The energy barriers for polarization switching in [100]-oriented $(HfO_2)_1/(CeO_2)_1$ are far lower than ~40 meV/atom in the $Pca2_1$ phase of HfO_2 [82]. In particular, the ultralow energy barrier of ~2.5 meV/atom in $(HfO_2)_1/(CeO_2)_1$ superlattice (a_{IP} being 5.34 Å) is also

significantly reduced, compared with ~7.6 meV/atom in the rhombohedral $Hf_{1.08}O_2$ [37]. This implies that the [100]-oriented $(HfO_2)_1/(CeO_2)_1$ superlattices enable the polarization switching via ultralow coercive electric field.

We next compute the electric polarization for the [100]-oriented $(HfO_2)_1/(CeO_2)_1$ superlattices. By symmetry, the [100]-oriented $(HfO_2)_1/(CeO_2)_1$ enables the P_x and P_z components of the polarization. Figure 2(c) shows the polarization of the [100]-oriented $(HfO_2)_1/(CeO_2)_1$ as a function of a_{IP}. At $a_{IP} = 5.30$ Å, the P_x and P_z are ~20.8 and ~22.1 μC/cm^2, yielding a total electric polarization of ~30.4 μC/cm^2 [83]. Varying a_{IP} from 5.24 to 5.34 Å decreases the total electric polarization from ~32.8 to ~25.8 μC/cm^2. The electric polarization values in the [100]-oriented $(HfO_2)_1/(CeO_2)_1$ superlattices are thus sizable, being comparable to those observed in various HfO_2-based ferroelectrics [e.g., ~22 μC/cm^2 in $Hf(Zr)_{1+x}O_2$ [37], ~34 μC/cm^2 in $Hf_{0.5}Zr_{0.5}O_2$ [30], and ~50 μC/cm^2 in Y-doped HfO_2 [16]].

Beyond $(HfO_2)_1/(CeO_2)_1$, hafnia-based ferroelectrics may also be achieved by creating the $(HfO_2)_1/(ZrO_2)_1$ superlattices—ZrO_2 crystallizing into the $P2_1/c$ phase (similar to monoclinic HfO_2) at ambient conditions [1]. In this regard, we explore the possibility for robust ferroelectricity in $(HfO_2)_1/(ZrO_2)_1$ superlattices via first-principles simulations. The polarizations for [001]- and [100]-oriented $(HfO_2)_1/(ZrO_2)_1$ superlattices (with no epitaxial constraints) are ~0.46 μC/cm^2 and ~2.68 μC/cm^2, respectively. Such polarization values for $(HfO_2)_1/(ZrO_2)_1$ superlattices are much smaller than those in the [100]-oriented $(HfO_2)_1/(CeO_2)_1$ superlattices. As a matter of fact, the ionic radius of Hf (0.83 Å) and Zr (0.84 Å) are very close to each other [84]. Achieving sizable polarization in monoclinic $(HfO_2)_1/(ZrO_2)_1$ superlattice thus seems unlikely.

Summary.—In summary, we demonstrate by symmetry analysis that the Hf sublattice in the monoclinic phase of HfO_2 presents three types of antipolar motions. These antipolar motions enable the creation of electric polarization in this monoclinic phase by forming the [100]- or [001]-oriented $(HfO_2)_1/(XO_2)_1$ superlattice ($X \neq$ Hf). Our first-principles calculations further predict the [100]-oriented $(HfO_2)_1/(CeO_2)_1$ superlattices as a new class of hafnia-based ferroelectrics. The ferroelectricity in $(HfO_2)_1/(CeO_2)_1$ superlattices is tunable by varying its in-plane lattice parameters (a_{IP}). In particular, our designated ferroelectric superlattice ($a_{IP} = 5.34$ Å) showcases a sizable electric polarization > 25 μC/cm^2 and an ultralow energy barrier at ~2.5 meV/atom, which is promising for the design of nonvolatile memory devices (e.g., ferroelectric random-access memory) with high integration and low power cost.

Note added.—During the peer review process, we became aware of a work [85] that mainly focuses on the ferroelectricity in various hafnia-based superlattices—being rooted in the ferroelectric orthorhombic phase of hafnia.

We acknowledge the support from the National Key Research and Development Program of China (Grant No. 2022YFA1402502) and the National Natural Science Foundation of China (Grants No. T2225013, No. 12274174, No. 52288102, and No. 12034009). L. B. acknowledges support from the Vannevar Bush Faculty Fellowship (VBFF) from the Department of Defense and Award No. DMR-1906383 from the National Science Foundation Q-AMASE-i Program (MonArk NSF Quantum Foundry). H. J. Z. thanks the "Xiaomi YoungScholar" Proiect. The authors acknowledge the support from the high-performance computing center of Jilin University. We also thank Professor Zuhuang Chen at Harbin Institute of Technology (Shenzhen) and Professor Yingfen Wei at Fudan University for valuable discussion.

*wyc@calypso.cn
†mym@jlu.edu.cn

[1] U. Schroeder, M. H. Park, T. Mikolajick, and C. S. Hwang, Nat. Rev. Mater. **7**, 653 (2022).
[2] B. Noheda, P. Nukala, and M. Acuautla, Nat. Mater. **22**, 562 (2023).
[3] T. S. Böscke, J. Müller, D. Bräuhaus, U. Schröder, and U. Böttger, Appl. Phys. Lett. **99**, 102903 (2011).
[4] O. Ohtaka, H. Fukui, T. Kunisada, T. Fujisawa, K. Funakoshi, W. Utsumi, T. Irifune, K. Kuroda, and T. Kikegawa, J. Am. Ceram. Soc. **84**, 1369 (2004).
[5] Y. Qi, S. Singh, C. Lau, F.-T. Huang, X. Xu, F. J. Walker, C. H. Ahn, S.-W. Cheong, and K. M. Rabe, Phys. Rev. Lett. **125**, 257603 (2020).
[6] L.-Y. Ma and S. Liu, Phys. Rev. Lett. **130**, 096801 (2023).
[7] R. He, H. Wu, S. Liu, H. Liu, and Z. Zhong, Phys. Rev. B **104**, L180102 (2021).
[8] K. Z. Rushchanskii, S. Blügel, and M. Ležaić, Phys. Rev. Lett. **127**, 087602 (2021).
[9] R. Materlik, C. Künneth, and A. Kersch, J. Appl. Phys. **117**, 134109 (2015).
[10] R. Batra, H. D. Tran, and R. Ramprasad, Appl. Phys. Lett. **108**, 172902 (2016).
[11] S. Liu and B. M. Hanrahan, Phys. Rev. Mater. **3**, 054404 (2019).
[12] T. Zhu, S. Deng, and S. Liu, Phys. Rev. B **108**, L060102 (2023).
[13] C.-K. Lee, E. Cho, H.-S. Lee, C. S. Hwang, and S. Han, Phys. Rev. B **78**, 012102 (2008).
[14] C. Liu, F. Liu, Q. Luo, P. Huang, X. X. Xu, H. B. Lv, Y. D. Zhao, X. Liu, and J. F. Kang, in *Proceedings of the 2018 IEEE International Electron Devices Meeting (IEDM)* (IEEE, New York, 2018), pp. 16.4.1–16.4.4.
[15] X. Xu, F.-T. Huang, Y. Qi, S. Singh, K. M. Rabe, D. Obeysekera, J. Yang, M.-W. Chu, and S.-W. Cheong, Nat. Mater. **20**, 826 (2021).

[16] Y. Yun, P. Buragohain, M. Li, Z. Ahmadi, Y. Zhang, X. Li, H. Wang, J. Li, P. Lu, L. Tao, H. Wang, J. E. Shield, E. Y. Tsymbal, A. Gruverman, and X. Xu, Nat. Mater. **21**, 903 (2022).

[17] X. Sang, E. D. Grimley, T. Schenk, U. Schroeder, and J. M. LeBeau, Appl. Phys. Lett. **106**, 162905 (2015).

[18] T. Shimizu, K. Katayama, T. Kiguchi, A. Akama, T. J. Konno, and H. Funakubo, Appl. Phys. Lett. **107**, 032910 (2015).

[19] P. Jiao, H. Cheng, J. Li, H. Chen, Z. Liu, Z. Xi, W. Ding, X. Ma, J. Wang, N. Zheng, Y. Nie, Y. Deng, L. Bellaiche, Y. Yang, and D. Wu, Appl. Phys. Rev. **10**, 031417 (2023).

[20] U. Schroeder, C. Richter, M. H. Park, T. Schenk, M. Pešić, M. Hoffmann, F. P. G. Fengler, D. Pohl, B. Rellinghaus, C. Zhou, C.-C. Chung, J. L. Jones, and T. Mikolajick, Inorg. Chem. **57**, 2752 (2018).

[21] X. Li, C. Li, Z. Xu, Y. Li, Y. Yang, H. Hu, Z. Jiang, J. Wang, J. Ren, C. Zheng, C. Lu, and Z. Wen, Phys. Status Solidi RRL **15**, 2000481 (2021).

[22] S. Zheng, Z. Zhao, Z. Liu, B. Zeng, L. Yin, Q. Peng, M. Liao, and Y. Zhou, Appl. Phys. Lett. **117**, 212904 (2020).

[23] T. Shiraishi, S. Choi, T. Kiguchi, T. Shimizu, H. Funakubo, and T. J. Konno, Appl. Phys. Lett. **114**, 232902 (2019).

[24] T. Shiraishi, S. Choi, T. Kiguchi, and T. J. Konno, Acta Mater. **235**, 118091 (2022).

[25] T. Shiraishi, T. J. Konno, and H. Funakubo, Appl. Phys. Lett. **120**, 132901 (2022).

[26] K. Hirai, T. Shiraishi, W. Yamaoka, R. Tsurumaru, Y. Inoue, and H. Funakubo, Jpn. J. Appl. Phys. **61**, SN1019 (2022).

[27] S. Estandía, N. Dix, J. Gazquez, I. Fina, J. Lyu, M. F. Chisholm, J. Fontcuberta, and F. Sánchez, ACS Appl. Electron. Mater. **1**, 1449 (2019).

[28] M. H. Park, H. J. Kim, Y. J. Kim, W. Lee, T. Moon, and C. S. Hwang, Appl. Phys. Lett. **102**, 242905 (2013).

[29] M. H. Park, H. J. Kim, Y. J. Kim, T. Moon, and C. S. Hwang, Appl. Phys. Lett. **104**, 072901 (2014).

[30] Y. Wei, P. Nukala, M. Salverda, S. Matzen, H. J. Zhao, J. Momand, A. S. Everhardt, G. Agnus, G. R. Blake, P. Lecoeur, B. J. Kooi, J. Íñiguez, B. Dkhil, and B. Noheda, Nat. Mater. **17**, 1095 (2018).

[31] P. Nukala, Y. Wei, V. de Haas, Q. Guo, J. Antoja-Lleonart, and B. Noheda, Ferroelectrics **569**, 148 (2020).

[32] P. Nukala, M. Ahmadi, Y. Wei, S. de Graaf, E. Stylianidis, T. Chakrabortty, S. Matzen, H. W. Zandbergen, A. Björling, D. Mannix, D. Carbone, B. Kooi, and B. Noheda, Science **372**, 630 (2021).

[33] S. Kang *et al.*, Science **376**, 731 (2022).

[34] S. S. Cheema *et al.*, Nature (London) **604**, 65 (2022).

[35] M. H. Park, H. J. Kim, G. Lee, J. Park, Y. H. Lee, Y. J. Kim, T. Moon, K. D. Kim, S. D. Hyun, H. W. Park, H. J. Chang, J.-H. Choi, and C. S. Hwang, Appl. Phys. Rev. **6**, 041403 (2019).

[36] D. Lehninger, A. Prabhu, A. Sünbül, T. Ali, F. Schöne, T. Kämpfe, K. Biedermann, L. Roy, K. Seidel, M. Lederer, and L. M. Eng, Adv. Phys. Res. **2**, 2200108 (2023).

[37] Y. Wang, L. Tao, R. Guzman, Q. Luo, W. Zhou, Y. Yang, Y. Wei, Y. Liu, P. Jiang, Y. Chen, S. Lv, Y. Ding, W. Wei, T. Gong, Y. Wang, Q. Liu, S. Du, and M. Liu, Science **381**, 558 (2023).

[38] E. D. Grimley, T. Schenk, X. Sang, M. Pešić, U. Schroeder, T. Mikolajick, and J. M. LeBeau, Adv. Electron Mater. **2**, 1600173 (2016).

[39] E. D. Grimley, T. Schenk, T. Mikolajick, U. Schroeder, and J. M. LeBeau, Adv. Mater. Interfaces **5**, 1701258 (2018).

[40] L. Yu, H. J. Zhao, P. Chen, L. Bellaiche, and Y. Ma, Nat. Commun. **14**, 8127 (2023).

[41] The $-[uvw]$ direction should be understood as the $[\bar{u}\,\bar{v}\,\bar{w}]$ crystallographic direction.

[42] In the following, the $[uvw]$-oriented $(HfO_2)_1/(XO_2)_1$ superlattice is referred to as the superlattice where the Hf and X ions are ordered by layer along the crystallographic $[uvw]$ direction.

[43] N. A. Benedek and C. J. Fennie, Phys. Rev. Lett. **106**, 107204 (2011).

[44] H. J. Zhao, J. Íñiguez, W. Ren, X. M. Chen, and L. Bellaiche, Phys. Rev. B **89**, 174101 (2014).

[45] J. M. Rondinelli and C. J. Fennie, Adv. Mater. **24**, 1961 (2012).

[46] A. T. Mulder, N. A. Benedek, J. M. Rondinelli, and C. J. Fennie, Adv. Funct. Mater. **23**, 4810 (2013).

[47] Materials Project, https://materialsproject.org/.

[48] A. Jain, S. P. Ong, G. Hautier, W. Chen, W. D. Richards, S. Dacek, S. Cholia, D. Gunter, D. Skinner, G. Ceder, and K. A. Persson, APL Mater. **1**, 011002 (2013).

[49] The first-principles calculated lattice parameter is 5.40 Å for bulk CeO_2.

[50] M. L. Gupta and S. Singh, J. Am. Ceram. Soc. **53**, 663 (1970).

[51] F. Zhang, C.-H. Chen, J. C. Hanson, R. D. Robinson, I. P. Herman, and S.-W. Chan, J. Am. Ceram. Soc. **89**, 1028 (2006).

[52] M. Yashima, H. Arashi, M. Kakihana, and M. Yoshimura, J. Am. Ceram. Soc. **77**, 1067 (1994).

[53] The phonon calculations further confirm the dynamical stabilities (at 300 K) for the [100]-oriented $(HfO_2)_1/(CeO_2)_1$ superlattices [see Fig. S3 of the Supplemental Material].

[54] See Supplemental Material, which includes Refs. [55–78], at http://link.aps.org/supplemental/10.1103/PhysRevLett.132.256801 for methods, Landau theory, and some numerical results.

[55] G. Kresse and J. Furthmüller, Phys. Rev. B **54**, 11169 (1996).

[56] G. Kresse and D. Joubert, Phys. Rev. B **59**, 1758 (1999).

[57] J. P. Perdew, A. Ruzsinszky, G. I. Csonka, O. A. Vydrov, G. E. Scuseria, L. A. Constantin, X. Zhou, and K. Burke, Phys. Rev. Lett. **100**, 136406 (2008).

[58] P. E. Blöchl, Phys. Rev. B **50**, 17953 (1994).

[59] G. Henkelman, B. P. Uberuaga, and H. Jónsson, J. Chem. Phys. **113**, 9901 (2000).

[60] G. Henkelman and H. Jónsson, J. Chem. Phys. **113**, 9978 (2000).

[61] Transition state tools for vasp, https://theory.cm.utexas.edu/vtsttools/index.html.

[62] R. D. King-Smith and D. Vanderbilt, Phys. Rev. B **47**, 1651 (1993).

[63] D. Orobengoa, C. Capillas, M. I. Aroyo, and J. M. Perez-Mato, J. Appl. Crystallogr. **42**, 820 (2009).

[64] J. M. Perez-Mato, D. Orobengoa, and M. I. Aroyo, Acta Crystallogr. Sect. A **66**, 558 (2010).
[65] B. J. Campbell, H. T. Stokes, D. E. Tanner, and D. M. Hatch, J. Appl. Crystallogr. **39**, 607 (2006).
[66] F. Knoop, N. Shulumba, A. Castellano, J. P. A. Batista, R. Farris, M. J. Verstraete, M. Heine, D. Broido, D. S. Kim, J. Klarbring, I. A. Abrikosov, S. I. Simak, and O. Hellman, J. Open Source Software **9**, 6150 (2024).
[67] O. Hellman, I. A. Abrikosov, and S. I. Simak, Phys. Rev. B **84**, 180301(R) (2011).
[68] O. Hellman, P. Steneteg, I. A. Abrikosov, and S. I. Simak, Phys. Rev. B **87**, 104111 (2013).
[69] O. Hellman and I. A. Abrikosov, Phys. Rev. B **88**, 144301 (2013).
[70] A. H. Romero, E. K. U. Gross, M. J. Verstraete, and O. Hellman, Phys. Rev. B **91**, 214310 (2015).
[71] Tdep, https://tdep-developers.github.io/tdep.
[72] H. T. Stokes, D. M. Hatch, and B. J. Campbell, FINDSYM, ISOTROPY Software Suite, https://iso.byu.edu.
[73] H. T. Stokes and D. M. Hatch, J. Appl. Crystallogr. **38**, 237 (2005).
[74] K. Momma and F. Izumi, J. Appl. Crystallogr. **44**, 1272 (2011).
[75] Seek-path, https://tools.materialscloud.org/seekpath.
[76] Y. Hinuma, G. Pizzi, Y. Kumagai, F. Oba, and I. Tanaka, Comput. Mater. Sci. **128**, 140 (2017).
[77] A. Togo and I. Tanaka, arXiv:1808.01590.
[78] J. D. Hunter, Comput. Sci. Eng. **9**, 90 (2007).
[79] The analysis regarding the [001]-oriented $(HfO_2)_1/(CeO_2)_1$ superlattice can be found in Sec. II of the SM.
[80] The intermediate $P2/c$ (respectively, $P2_1/c$) phase can be obtained by the linear interpolation between the O_{100} initial state and the O'_{100} (respectively, O''_{100}) final state. The ratio for such a linear interpolation is $1:1$.
[81] See https://theory. cm.utexas.edu/vtsttools/neb.html for the nudged elastic band algorithm. This algorithm determines the possible transition paths between initial and final states, with the minimum energy barriers.
[82] T. D. Huan, V. Sharma, G. A. Rossetti, and R. Ramprasad, Phys. Rev. B **90**, 064111 (2014).
[83] We further examine the electric polarization for the "bulk" [100]-oriented $(HfO_2)_1/(CeO_2)_1$ superlattice (i.e., without epitaxial constraints). The polarization values for such a superlattice are $\sim$21.0 $\mu C/cm^2$ for P_x and $\sim$22.4 $\mu C/cm^2$ for P_z.
[84] R. D. Shannon, Acta Crystallogr. Sect. A **32**, 751 (1976).
[85] B. Mukherjee, N. S. Fedorova, and J. Íñiguez González, arXiv:2401.05288.